

## Article

# Heat and Mass Transport Analysis of MHD Rotating Hybrid Nanofluids Conveying Silver and Molybdenum Di-Sulfide Nano-Particles under Effect of Linear and Non-Linear Radiation

Ali Hassan <sup>1,\*</sup>, Azad Hussain <sup>1</sup>, Mubashar Arshad <sup>1</sup>, Jan Awrejcewicz <sup>2</sup>, Witold Pawlowski <sup>3</sup>, Fahad M. Alharbi <sup>4</sup> and Hanen Karamti <sup>5</sup>

<sup>1</sup> Department of Mathematics, University of Gujrat, Gujrat 50700, Pakistan

<sup>2</sup> Department of Automation, Biomechanics and Mechatronics, Lodz University of Technology, 90-924 Lodz, Poland

<sup>3</sup> Institute of Machine Tools and Production Engineering, Lodz University of Technology, 90-924 Lodz, Poland

<sup>4</sup> Department of Mathematics, Al-Qunfudah University College, Umm Al-Qura University, Mecca 24382, Saudi Arabia

<sup>5</sup> Department of Computer Sciences, College of Computer and Information Sciences, Princess Nourah bint Abdulrahman University, P.O. Box 84428, Riyadh 11671, Saudi Arabia

\* Correspondence: muhammadali0544@gmail.com



**Citation:** Hassan, A.; Hussain, A.; Arshad, M.; Awrejcewicz, J.; Pawlowski, W.; Alharbi, F.M.; Karamti, H. Heat and Mass Transport Analysis of MHD Rotating Hybrid Nanofluids Conveying Silver and Molybdenum Di-Sulfide Nano-Particles under Effect of Linear and Non-Linear Radiation. *Energies* **2022**, *15*, 6269. <https://doi.org/10.3390/en15176269>

Academic Editors: Giuseppe Pascazio and Fateh Mebarek-Oudina

Received: 13 July 2022

Accepted: 24 August 2022

Published: 28 August 2022

**Publisher's Note:** MDPI stays neutral with regard to jurisdictional claims in published maps and institutional affiliations.



**Copyright:** © 2022 by the authors. Licensee MDPI, Basel, Switzerland. This article is an open access article distributed under the terms and conditions of the Creative Commons Attribution (CC BY) license (<https://creativecommons.org/licenses/by/4.0/>).

**Abstract:** This article is an attempt to explore the heat transfer features of the steady three-dimensional rotating flow of magneto-hydrodynamic hybrid nanofluids under the effect of nonlinear radiation over the bi-directional stretching surface. For this purpose, two different nano-particles, namely silver (Ag) and molybdenum di-sulfide (MoS<sub>2</sub>), were selected. Three different conventional base fluids were utilized to form desired hybrid nanofluids such as water (H<sub>2</sub>O), engine oil (EO), and ethylene glycol (EG). We obtained steady three-dimensional highly nonlinear partial differential equations. These highly nonlinear partial differential equations cannot be solved analytically, so these equations were handled in MATLAB with the BVP-4C technique with convergence tolerance at 10<sup>-6</sup>. The graph depicts the effect of the magnetization effect, thermal radiation, and stretching ratio on rotating hybrid nanofluids. Additionally, the impact of thermal radiation on the heat coefficient of three different hybrid nanofluids is being investigated. The augmentation in magnetization decreases the primary velocity, whereas the increment in radiation enhances the primary velocity. The stretching ratio and the presence of higher magnetic forces increase the temperature profile. The concentration profile was enhanced with an increment in the magnetic field, stretching, and rotation ratio. The maximum Nusselt number was achieved for the Ag-MoS<sub>2</sub>/EO hybrid nanofluid. It was concluded that augmentation in nonlinear radiation enhances the heat transfer coefficient for the examined cases (I) and (II) of the hybrid nanofluids. The Nusselt number doubled for both the examined cases under nonlinear radiation. Moreover, it was discovered that Ag-MoS<sub>2</sub>/water produced the best heat transfer results under nonlinear radiation. Therefore, the study recommends more frequent exploration of hybrid nanofluids (Ag-MoS<sub>2</sub>/water) when employing nonlinear radiation to analyze the heat transfer coefficient.

**Keywords:** hybrid nano-particles; MHD flow; Rosseland radiation and stretching surface; water; engine oil; ethylene glycol; silver and molybdenum Di-sulfide

## 1. Introduction

The heat exchange phenomena have been associated with numerous industrial applications. The impact and effectiveness of MEMS and thermal devices can be significantly improved using nanofluid heat transfer features. The loss in thermal energy can be reduced by enhancing the heat efficiency, thus minimizing the production cost. The hybrid nanofluids have greater rates of heat transfer when compared to nanofluids. An undeniable

factor that contributes to high heat transfer rates is the high thermal conductivity of hybrid nanofluids. The hybrid nanofluids distributed in hybrid-based fluids have even better outcomes [1–5].

On engine oil-based hybrid nanofluids, Jamshed et al. [6] discussed amplified entropy and relative probe. Ouni et al. [7] conducted a thermal case study on hybrid nanofluids flowing in a parabolic trough collector to investigate the solar water pump efficiency. Ghadikolaei et al. [8] explored hybrid nanofluids distributed in a hybrid base fluid under thermal radiation to study the natural convection of MHD flow. Hayat and Nadeem [9] discussed hybrid nanofluids for heat transfer enhancement. Hayat et al. [10] elaborated on a hybrid nanofluid with radiation and slip boundary effects for rotating flow. Ghadikolaei et al. [11] analyzed the mixture-based hybrid nanofluids over a spinning cone for the nanoparticle shape factor. Humnic and Humnic [12] described hybrid nanofluid heat transfer for application in different fields. Mebarek-Oudina et al. [13] investigated the heat transfer in a magnetized non-Newtonian fluid with a discrete heat source. Marzougui et al. [14] demonstrated the entropy generation and heat transfer of the copper/water nanofluid in a porous lid-driven cavity with a magnetic field. Khan et al. [15] studied the magneto convection with hybrid nanofluids through a stretching/shrinking wedge to analyze the stability of hybrid fluids. Hassan et al. [16] examined the hybrid nanoparticles for thermal enhancement over a rotating system for a prescribed wall temperature case. Hassan et al. [17] explained the heat transfer in a hybrid nanofluid under the effects of magnetic fields and Rosseland radiation. Hybrid nanofluids have been examined by a plethora of scientists in recent years. Here are some notable articles for knowledge purposes [18–22].

Fluids are utilized as heat exchangers in heat transfer materials and equipment. The low thermal conductivity does not help to transfer heat more effectively. Thus, nanometer metallic or non-metallic particles were proposed to be distributed in conventional fluids (water, ethylene glycol, and engine oil) to enhance the heat transfer in industrial applications. The term “nanofluid” was coined, thermal conductivity was highly improved, and it revolutionized this particular research area [23]. Jamshed et al. [24] conducted a thorough investigation into engine oil-based Casson fluid and its thermal properties in a solar trough collector. Asogwa et al. [25] investigated  $\text{Al}_2\text{O}_3$  and CuO nanoparticles over an exponentially accelerated radiative Riga plate surface with heat transport. Shahzad et al. [26] discussed the thermal features of Oldroyd-B copper and molybdenum disulfide in engine oil-based nanofluids. Sheikholeslami and Ellahi [27] investigated three-dimensional mesoscopic simulation of magnetic field effects on the natural convection of nanofluid.

Majeed et al. [28] investigated the heat transfer in ferro-magnetic viscoelastic fluid flow over a stretching surface with a suction effect. The magnetic dipole effect on the heat transfer analysis of Jeffery fluid over a stretching surface in the presence of suction and blowing effects was discussed by Zeeshan and Majeed [29]. Hussain et al. [30] introduced a model for time-dependent flow that focused on heat transportation enrichment. Nadeem et al. [31] explained the exponentially stretching surface for the boundary layer flow of nanofluid, and Raza et al. [32] investigated the non-Newtonian flow in a converging/diverging channel with Rosseland radiation. Raza et al. [33] discussed the magneto-hydrodynamic flow of a nanofluid in a channel with the shape effect of nanoparticles. Mebarek-Oudina et al. [34] introduced the numerical modeling of hydrodynamic stability in a vertical annulus with different heat source lengths. Chabani et al. [35] explored the magneto-hydrodynamic flow in a triangular enclosure with zigzags and elliptical obstacles. Laouira et al. [36] described the heat transfer of a nanofluid in a horizontal channel with a heat source of different lengths. Reddy et al. [37] studied magneto-hydrodynamic boundary layer flow with thermal slip, radiation, and slip velocity for heat and mass transfer in the Williamson nanofluid. Choudhari et al. [38] analyzed third grade fluid for inclined peristaltic motion with wall slip and variable fluid properties. Readers are referred to the following articles for greater knowledge [39–46].

MHD explores electrically conducting fluids. Generally, its effects on flow stream and heat transfer are prescribed in the form of joule heating and Lorentz force. In fact, the

applied magnetic field in the fluid decreases the fluid's flow motion, but a force resistance is created between electric and magnetic fields with stream layers as the temperature shifts. The Lorentz force acts in the opposite direction to the flow motion, which reduces the flow speed generated through the magnetic field [47,48].

Magneto-hydrodynamics describes the magnetic attributes of electrically conducting fluids. The generated resistive force due to magneto-hydrodynamics is termed the Lorentz force. Its other effects include joule heating, which effects the motion profile, heat and mass transfer of moving fluids. Raptis et al. [49] investigated the impact of radiation on MHD flow. Nadeem et al. [50] explored the Casson fluid over an exponentially shrinking sheet for MHD flow. Sarada et al. [51] studied the effect of magneto-hydrodynamics on heat transfer in non-Newtonian fluids over stretching surfaces with local thermal non-equilibrium conditions. Mishra et al. [52] discussed the free convective micro-polar fluid flow with a heat source over a stretching surface. Abo-Dahab et al. [53] examined the MHD Casson fluid over an extending surface with suction and injection effects embedded in a porous medium. Hamrelaine et al. [54] analyzed the MHD Jeffery Hemal system with suction and injection effects with the homotopy analysis method. Shafiq et al. [55] conducted a stability analysis of water's B nanofluid over the Riga surface. Hussain et al. [56] described the impact of nonlinear thermal radiation on MHD three-dimensional rotating flow over a stretching surface. Zainal et al. [57] studied unsteady EMHD stagnation point flow over a stretching/shrinking sheet in a hybrid nanofluid. The MHD flow has been discussed under different applied effects by a plethora of researchers. For some notable mentions, please see [58–61]. Hosseini et al. [62] presented the entropy analysis of nanofluid convection considering the solid heat generation in a heated porous micro-channel with magneto-hydrodynamic phenomena. Sheikholeslami et al. [63] conducted the second law analysis for the twisted tube tabulators inside a circular duct to investigate the turbulent nanofluid flow.

In the present study, the magneto-hydrodynamic flow of hybrid nanofluids under the effect of nonlinear radiation was investigated over a stretching surface. The motivation behind the study was to explore the newly discovered nanofluid category termed as a hybrid nanofluid. The novelty of the work was to address three different hybrid nanofluids under nonlinear thermal radiation for the evaluation of the heat transfer coefficient in the magneto-hydrodynamic flow over a linearly extending surface. In our study, we selected silver (Ag) and molybdenum di-sulfide (Ag-MoS<sub>2</sub>) as two different nanoparticles of a nanometer size to constitute our desired hybrid nanofluid. To obtain the different hybrid nanofluids, we chose three distinct base fluids, namely water, engine oil, and ethylene glycol, to host our nanoparticles. For instance, to obtain a hybrid nanofluid, first the silver nanoparticle is dispersed in the host base liquid, for instance, water, and then, as a product, we have a Ag/water nanofluid. The desired hybrid nanofluid is achieved when another nanoparticle such as molybdenum di-sulfide (MoS<sub>2</sub>) is distributed in an already formed nanofluid (Ag/water) to form a hybrid nanofluid Ag-MoS<sub>2</sub>/water. The other two hybrid nanofluids were achieved following a similar procedure to acquire a hybrid nanofluid, namely, Ag-MoS<sub>2</sub>/engine oil and Ag-MoS<sub>2</sub>/ethylene glycol. The highly nonlinear partial differential equations were tackled numerically with the BVP-4c technique in MATLAB. The influence of different study parameters such as magnetization force, thermal radiation, and stretching ratio on distinct study profiles is discussed for the three selected hybrid nanofluids. The linear and nonlinear impact of radiation on the heat transfer coefficient was analyzed. The heat shift examined in the study is illustrated and suggests that exploitation of hybrid nanofluids at industrial levels can vastly improve the thermal energy shift and reduce the production expenditure. The following research questions elaborate the need to study the present formulated problem.

1. What is the effect of thermal radiation on different profiles, namely, velocities, temperature, and concentration of (Ag-MoS<sub>2</sub>/H<sub>2</sub>O, Ag-MoS<sub>2</sub>/EO, Ag-MoS<sub>2</sub>/EG) hybrid nanofluids?
2. Which hybrid nanofluid combination produces low shear stress rates and high heat transfer rates in the presence of high resistive force?

3. What is the effect of nonlinear radiation on the heat transfer attributes of the two examined cases such as Ag-MoS<sub>2</sub>/H<sub>2</sub>O and Ag-MoS<sub>2</sub>/EG?
4. What is the impact of the rotation and stretching ratio on the three-dimensional hybrid nanofluid flow motion, temperature, and concentration profiles?
5. Which of all of the examined hybrid nanofluids (Ag-MoS<sub>2</sub>/H<sub>2</sub>O, Ag-MoS<sub>2</sub>/EO, Ag-MoS<sub>2</sub>/EG) produces higher heat and mass transfer?

## 2. Mathematical Formulation

Consider the magneto-hydrodynamic viscous incompressible three-dimensional flow of hybrid nanofluids over a linear stretching surface. The linear stretching velocities  $U_w(x) = u = ax$  and  $V_w(x) = v = by$  and along the  $x$ -axis and  $y$ -axis, respectively. The fluid occupies the space  $Z > 0$ , and the flow is induced by linear stretching at different velocities. A magnetic field  $B_0$  is applied in the normal direction to the sheet in the presence of Rosseland radiation. Figure 1 shows the geometry of the problem.

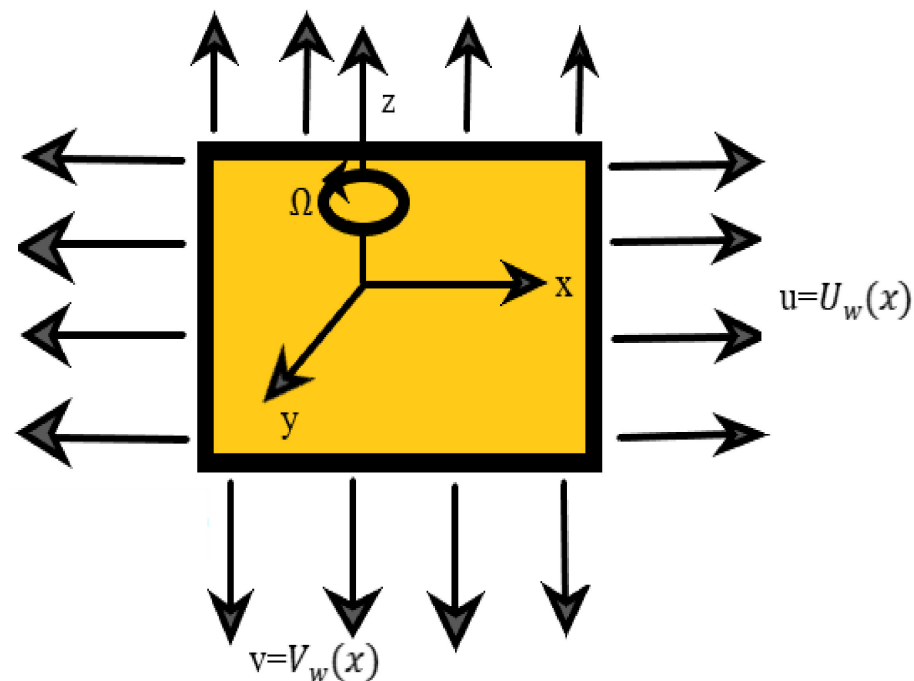


**Figure 1.** The geometry and coordinate system.

The nano-sized particles considered for analysis were Ag and MoS<sub>2</sub> with different fluids as the base liquid. We considered Ag ( $\varphi_1$ ) and MoS<sub>2</sub> ( $\varphi_2$ ) as initially Ag nano-particles with a solid volume fraction of 0.005 vol (which was kept unaltered throughout the problem analysis) a distributed in the three different base fluids to form the nanofluids Ag–water, Ag–engine oil, and Ag–ethylene glycol. The desired set of hybrid nanofluids (Ag-MoS<sub>2</sub>/H<sub>2</sub>O, Ag-MoS<sub>2</sub>/EO, Ag-MoS<sub>2</sub>/EG) was obtained by scattering the second nano-particle MoS<sub>2</sub> with a different volume fraction into the already formed nanofluid. The hybrid nanofluid rotates around a vertical axis and the angular velocity  $\omega^*$  is kept constant. Hussain et al. [41] formulated the three-dimensional flow of engine oil-based nanofluids (TiO<sub>2</sub> and ZnO) in the absence of externally applied effect and species continuity. Recently, Arshad et al. [43] investigated distinct nanofluids over an exponentially stretching surface in the absence of body force and concentration profile. Hussain et al. [56] examined nanofluid 3D flow under the combined effect of the magnetic field and linear radiation, but they did not incorporate the species transport. In our study, we incorporated the species continuity equation, linear, nonlinear radiation, and magnetization force to analyze the three different hybrid nanofluids. Considering all the assumptions above-mentioned, along with boundary layer approximation, the governing equations such as

continuity, conservation of momentum, energy equation, and concentration equations are given as follows.

### 2.1. Equation of Continuity

The continuity equation for the viscous in-compressible three dimensional steady flow obtained is given as:

$$\frac{\partial u}{\partial x} + \frac{\partial v}{\partial y} + \frac{\partial w}{\partial z} = 0. \quad (1)$$

### 2.2. Momentum Equations

The magnetic field relation is incorporated into the horizontal and vertical momentum equations. The momentum equations in said directions is defined as:

$$u \frac{\partial u}{\partial x} + v \frac{\partial u}{\partial y} + w \frac{\partial u}{\partial z} - 2\omega^* v = \nu_{hmf} \frac{\partial^2 u}{\partial z^2} - \frac{\sigma_{hmf} B_0^2}{\rho_{hmf}} u, \quad (2)$$

$$u \frac{\partial v}{\partial x} + v \frac{\partial v}{\partial y} + w \frac{\partial v}{\partial z} + 2\omega^* u = \nu_{hmf} \frac{\partial^2 v}{\partial z^2} - \frac{\sigma_{hmf} B_0^2}{\rho_{hmf}} v. \quad (3)$$

### 2.3. Energy Relation without Rosseland Expression of Thermal Radiation

The relation of energy without relation Rosseland thermal radiation is defined as:

$$u \frac{\partial T}{\partial x} + v \frac{\partial T}{\partial y} + w \frac{\partial T}{\partial z} = \alpha_{hmf} \frac{\partial^2 T}{\partial z^2} - \frac{1}{(\rho C_p)_{hmf}} \frac{\partial(q_r)}{\partial z}. \quad (4)$$

### 2.4. Species Continuity Equation

The three dimensional nano-particles concentration profile is defined as:

$$u \frac{\partial C}{\partial x} + v \frac{\partial C}{\partial y} + w \frac{\partial C}{\partial z} = D_m \frac{\partial^2 C}{\partial z^2}. \quad (5)$$

With relevant boundary conditions:

$$u = U_w = ax, v = V_w = by, w = 0, C = C_W \text{ and } T = T_w \text{ at } z = 0, \quad (6)$$

$$u = 0, v = 0, w = 0, C \rightarrow C_\infty \text{ and } T \rightarrow T_\infty \text{ at } z \rightarrow \infty. \quad (7)$$

In the above equations,  $(u, v, w)$  are the velocity components in the respective directions;  $\omega^*$  is the rotational velocity of rotating flow;  $B_0$  is the applied magnetic field in the normal direction;  $T$  denotes the temperature;  $(q_r)$  expresses the Rosseland expression;  $\sigma_{hmf}$  is the electrical conductivity of the hybrid nanofluid;  $(\rho C_p)_{hmf}$  is the heat capacity at constant pressure for the hybrid nanofluids;  $C$  describes the concentration of species;  $\alpha_{hmf}$  is the thermal diffusivity of the hybrid nanofluid;  $D_m$  denotes the mass diffusivity;  $T_w, T_\infty$  are the surface and ambient temperatures  $C_w, C_\infty$  and show the surface and ambient concentration stages, respectively. Here, we introduce the following set of the similarity transforms that were utilized in this problem and can be found in the studies of [43,56,58,59].

$$u = axp'(\eta), v = ayq'(\eta), w = -\sqrt{av_f} [p(\eta) + q(\eta)], \quad (8)$$

$$\eta = z\sqrt{\frac{a}{v_f}}, r(\eta) = \frac{T-T_\infty}{T_w-T_\infty}, \varphi(\eta) = \frac{C-C_\infty}{C_w-C_\infty}.$$

### 2.5. Final Energy Relation

The radiative heat flux  $q_r$ , more commonly known as the Rosseland approximation, is defined as  $q_r = -\frac{4\sigma^*}{3K^*} \frac{\partial T^4}{\partial z}$ ;  $\sigma^*$  is the Stefan Boltzmann constant;  $K^*$  is the absorption coefficient; and  $k_f$  is the thermal conductivity of the base liquid. Assuming the temperature difference is low, the expansion of  $T^4$  in terms of  $T_\infty$  with the help of the Taylor series is as follows:

$$T^4 \approx 4TT_\infty^3 - 3T_\infty^4 \dots \dots \dots \tag{9}$$

After the replacement of heat flux  $q_r$  and temperature expansion (9), the energy Equation (4) will become

$$u \frac{\partial T}{\partial x} + v \frac{\partial T}{\partial y} + w \frac{\partial T}{\partial z} = \alpha_{hnf} \frac{\partial^2 T}{\partial z^2} + \frac{1}{(\rho C_p)_{hnf}} \frac{16\sigma^* T_\infty^3}{3K^*} \frac{\partial^2 T}{\partial z^2} \tag{10}$$

Now, as we are analyzing the linear and nonlinear effects of radiation, it is worth noting here that we can use the radiation relation defined in Equation (17) for the linear impact of radiation on magnetized flow. Additionally, when we implement nonlinear radiation, the temperature will become  $T = T_\infty [1 + (r_w - 1)r]$ , where  $r_w$  is known as the temperature difference ratio, defined as  $r_w = \frac{T_w}{T_\infty}$ . Now, the governing flow equations of momentum, energy, and concentration (2), (3), (5), (10), respectively, will take the following form after utilizing the above-mentioned similarity transform.

$$p'''(\eta) - (1 - \varphi_1)^{2.5}(1 - \varphi_2)^{2.5} \left\{ (1 - \varphi_2) \left[ (1 - \varphi_1) + \varphi_1 \left( \frac{\rho_{s1}}{\rho_f} \right) \right] + \varphi_2 \left( \frac{\rho_{s2}}{\rho_f} \right) \right\} \left\{ [p'(\eta)]^2 - p''(\eta) [p(\eta) + q(\eta)] - 2\lambda \delta q'(\eta) \right\} - (1 - \varphi_1)^{2.5}(1 - \varphi_2)^{2.5} M^2 p'(\eta) = 0, \tag{11}$$

$$q'''(\eta) - (1 - \varphi_1)^{2.5}(1 - \varphi_2)^{2.5} \left\{ (1 - \varphi_2) \left[ (1 - \varphi_1) + \varphi_1 \left( \frac{\rho_{s1}}{\rho_f} \right) \right] + \varphi_2 \left( \frac{\rho_{s2}}{\rho_f} \right) \right\} \left\{ [q'(\eta)]^2 - q''(\eta) [p(\eta) + q(\eta)] - 2\lambda \delta p'(\eta) \right\} - (1 - \varphi_1)^{2.5}(1 - \varphi_2)^{2.5} M^2 q'(\eta) = 0, \tag{12}$$

$$\frac{1}{Pr} * \frac{r''(\eta)}{\left( (1 - \varphi_2) \left\{ (1 - \varphi_1) + \varphi_1 \left[ \frac{(\rho C_p)_{s1}}{(\rho C_p)_f} \right] \right\} + \varphi_2 \left[ \frac{(\rho C_p)_{s2}}{(\rho C_p)_f} \right] \right)} \left[ \frac{k_{hnf}}{k_f} - Rd(1 + (r_w - 1)r)^3 + (p + q)r' = 0 \right], \tag{13}$$

$$\varphi''(\eta) - Sc [\varphi - \varphi'(p + q)] = 0. \tag{14}$$

Now, the transformed boundary conditions are as follows:

$$p = 0, p' = 1, q = 0, q' = \gamma, r = 1 \text{ and } \varphi = 1 \text{ at } \eta = 0, \tag{15}$$

$$p' = 0, q' = 0, r = 0 \text{ and } \varphi = 0 \text{ at } \eta = \infty. \tag{16}$$

### 2.6. Non-Dimensional Quantities

The non-dimensional quantities of the present problem are defined and presented. These include the stretching ratio  $\gamma$ , rotational ratio of flow  $\lambda$ , magnetic field parameter  $M^2$ , Prandtl number  $pr$ , and thermal radiation parameter  $Rd$ . These dimensionless relations are defined as follows:

$$\gamma = \frac{b}{a}, \lambda = \frac{\omega^*}{a}, M^2 = \frac{\sigma B_0^2}{a\rho_f} \text{ and } Pr = \frac{k_f}{(\mu C_p)_f}, Rd = \frac{16\sigma^* T_\infty^3}{3K^* k_f}. \tag{17}$$

The shear stress rates in the x and y directions  $(C_{fx}, C_{fy})$ ; Nusselt  $Nu_x$  and Sherwood  $Sh_x$  numbers are the quantities of physical and engineering interest. The quantities in dimensional form are defined as follows:

$$C_{fx} = \frac{\mu_{hnf} \left( \frac{\partial u}{\partial z} \right)_{z=0}}{\rho_f (u)^2}, C_{fy} = \frac{\mu_{hnf} \left( \frac{\partial v}{\partial z} \right)_{z=0}}{\rho_f (u)^2}, \tag{18}$$

$$Nu_x = -\frac{x}{(T_w - T_\infty)} \left[ \frac{k_{hmf}}{k_f} + Rdr_w^3 \right] \left( \frac{\partial T}{\partial z} \right)_{z=0}, \quad Sh_x = -\frac{[\rho_f D \left( \frac{\partial C}{\partial z} \right)]_{z=0}}{(C_w - C_\infty)}. \quad (19)$$

The dimensionless form of the above quantities is given as follows:

$$Re^{1/2} C_{fx} = \frac{1}{(1 - \varphi_1)^{2.5} (1 - \varphi_2)^{2.5}} p''(0), \quad \delta^{-1} Re^{1/2} C_{fy} = \frac{1}{(1 - \varphi_1)^{2.5} (1 - \varphi_2)^{2.5}} q''(0), \quad (20)$$

$$Re^{-1/2} Nu_x = -\left[ \frac{k_{hmf}}{k_f} + Rdr_w^3 \right] r'(0), \quad Sh Re_x^{-\frac{1}{2}} = -\varphi'(0). \quad (21)$$

The Reynolds number is defined as follows:

$$Re = \frac{U_w x}{\nu_f}. \quad (22)$$

### 3. Numerical Solution

Different numerical methods have been utilized by researchers to study the hybrid nanofluids. Jamshed et al. [6,7] investigated HNF with the Keller Box method, Ghadikolaie et al. [8] explored HNF with Rung Kutt-4, and Hamrelaine et al. [54] employed the homotopy analysis method to study HNF. In this paper, we used the boundary value problem technique, more commonly known as the BVP-4c solver, in MATLAB. For this purpose, we introduced our own supposition set of Equations (23)–(34) to convert the highly nonlinear set of partial differential equations into first-order ordinary differential Equations (25)–(34), along with the boundary conditions (39) and (40). The set of our own suppositions is given as follows:

$$p' = y_1, \quad p'' = y_2, \quad p''' = y_3, \quad p'''' = y_3', \quad q = y_4, \quad q' = y_5, \quad q'' = y_6, \quad q''' = y_6', \quad (23)$$

$$r = y_7, \quad r' = y_8, \quad r'' = y_8', \quad \varphi = y_9, \quad \varphi' = y_{10}, \quad \varphi'' = y_{10}'. \quad (24)$$

Using the above stated suppositions, Equations (11)–(14), along with suitable boundary Equations (15) and (16), will transform into the following set of the first-order differential equations given as follows:

$$y_1' = y_2 \quad (25)$$

$$y_2' = y_3 \quad (26)$$

$$y_3' = AB \left\{ (y_2)^2 - y_3(y_1 + y_2) - 2\lambda\delta y_5 \right\} + M^2 A y_2, \quad (27)$$

$$y_4' = y_5 \quad (28)$$

$$y_5' = y_6 \quad (29)$$

$$y_6' = AB \left\{ (y_5)^2 - y_6(y_1 + y_4) - 2\lambda\delta y_6 \right\} + M^2 A y_5, \quad (30)$$

$$y_7' = y_8 \quad (31)$$

$$y_8' = -\left( \frac{pr * y_8 * (y_1 + y_4) C}{\left\{ D - Rd(1 + (r_w - 1)y_7)^3 \right\}} \right), \quad (32)$$

$$y_9' = y_{10} \quad (33)$$

$$y_{10}' = Sc[y_9 - y_{10}(y_1 + y_4)]. \quad (34)$$

Here, we define the properties of hybrid nanofluids utilized in the above ordinary differential equations. These include the viscosity of the HNF, the density of the HNF, the heat capacity of the HNF and the thermal conductivity of the HNF. Table 1 gives shear stress rates of HNF. Table 2 provide numeric data for Nusselt and Sherwood numbers.

Table 3 shows comparison of Nusselt number for two cases. The complete relations of these properties are defined in Table 4.

$$A = (1 - \varphi_1)^{2.5}(1 - \varphi_2)^{2.5}, \tag{35}$$

$$B = [(1 - \varphi_2)[(1 - \varphi_1) + \varphi_1(\frac{\rho_{s1}}{\rho_f})] + \varphi_2(\frac{\rho_{s2}}{\rho_f})], \tag{36}$$

$$C = (1 - \varphi_2) \left\{ \left\{ (1 - \varphi_1) + \varphi_1 \left[ \frac{(\rho C_p)_{s1}}{(\rho C_p)_f} \right] \right\} + \varphi_2 \left[ \frac{(\rho C_p)_{s2}}{(\rho C_p)_f} \right] \right\}, \tag{37}$$

$$D = \left( \frac{k_{s2} + (n - 1)k_{bf} - (n - 1)\varphi_2(k_{bf} - k_{s2})}{k_{s2} + (n - 1)k_{bf} + \varphi_2(k_{bf} - k_{s2})} * \frac{k_{s1} + (n - 1)k_f - (n - 1)\varphi_1(k_f - k_{s1})}{k_{s1} + (n - 1)k_f + \varphi_1(k_f - k_{s1})} \right). \tag{38}$$

The boundary conditions of the present problem are as follows:

$$y_0(1) = 0, y_0(2) = 1, y_0(5) = \gamma, y_0(7) = 1, y_0(9) = 1, \tag{39}$$

$$y_\infty(2) = 0, y_\infty(5) = 0, y_\infty(7) = 0, y_\infty(9) = 0. \tag{40}$$

**Table 1.** The skin friction ( $Cf_x, Cf_y$ ) results for the Ag-MoS<sub>2</sub>/H<sub>2</sub>O, Ag-MoS<sub>2</sub>/EO, Ag-MoS<sub>2</sub>/EG hybrid nanofluids.

				Ag-MoS <sub>2</sub> /Water		Ag-MoS <sub>2</sub> /EG		Ag-MoS <sub>2</sub> /EO	
$\varphi_1 = \varphi_2 = 0.05$				Pr = 6.2, Rd = 2.0		Pr = 23.50, Rd = 0.7		Pr = 6450, Rd = 1.2	
$\delta$	M	$\lambda$	$\gamma$	$Cf_x$	$Cf_y$	$Cf_x$	$Cf_y$	$Cf_x$	$Cf_y$
0.5	2	0.5	0.5	-2.08642	-1.30201	-1.99174	-1.24784	-6.58372	-0.175694
1				-2.08642	-1.30201	-1.99174	-1.24784	-6.58372	-0.175694
1	0.5	0.5	0.5	-1.53642	-1.03705	-1.31708	-0.932818	-5.50614	-0.145622
	1			-1.38102	-0.962711	-1.10318	-0.836186	-5.21681	-0.137422
0.5	1	0.6	0.5	-1.45668	-1.22153	-1.22695	-1.1239	-5.49056	-0.170364
		0.8		-1.50873	-1.09561	-1.28519	-0.993087	-5.50078	-0.153541
0.5	0.5	0.8	0.4	-1.29796	-1.15215	-1.00707	-1.0404	-5.20079	-0.162488
			0.5	-1.33268	-0.903353	-1.04699	-0.807836	-4.7511	-2.91562

**Table 2.** The Nusselt and Sherwood number ( $Nu_x, Sh_x$ ) results for the Ag-MoS<sub>2</sub>/H<sub>2</sub>O, Ag-MoS<sub>2</sub>/EO, Ag-MoS<sub>2</sub>/EG hybrid nanofluids.

				Ag-MoS <sub>2</sub> /Water		Ag-MoS <sub>2</sub> /EG		Ag-MoS <sub>2</sub> /EO	
$\varphi_1 = \varphi_2 = 0.05,$				Pr = 6.2, Rd = 2.0		Pr = 23.50, Rd = 0.7		Pr = 6450, Rd = 1.2	
$\delta$	M	$\lambda$	$\gamma$	$Nu_x$	$Sh_x$	$Nu_x$	$Sh_x$	$Nu_x$	$Sh_x$
0.5	2	0.5	0.5	9.58768	1.23465	8.81935	0.896578	10.8036	1.69725
1				9.58768	1.15701	8.81935	0.764266	10.8036	1.37308
1	0.5	0.5	0.5	8.87352	1.24101	8.97532	0.914744	10.8105	1.7075
	1			8.67011	1.2429	9.02376	0.921284	10.8123	1.71031
	1	0.6	0.5	8.93214	1.16303	8.96173	0.783724	10.8104	0.762583
		0.8		8.89092	1.16344	8.97152	0.784494	10.8105	0.762601
0.5	0.5	0.8	0.4	8.73251	1.16495	9.00894	0.790839	10.8123	0.996989
			0.5	9.20455	1.1598	8.70167	0.782954	12.6403	1.06938

**Table 3.** The comparison of the Nusselt number ( $Nu_x$ ) results for the Ag-MoS<sub>2</sub>/H<sub>2</sub>O, Ag-MoS<sub>2</sub>/EG hybrid nanofluids.

Case1 = Ag-MoS <sub>2</sub> /Water Case2 = Ag-MoS <sub>2</sub> /EG				Rd = 3.0 Nonlinear Radiation			
				$r_{w} = 1.5$		$r_{w} = 2.0$	
$\delta$	$M$	$\lambda$	$\gamma$	case1	case 2	case 1	case 2
0.5	2	0.5	0.5	1.62791	0.00154652	3.53586	0.0227284
1				1.62791	0.00154652	3.53586	0.0227284
1	0.5	0.5	0.5	0.879007	0.0000542623	2.58821	0.00509825
	1			0.752469	0.0000234311	2.30749	0.00293049
	1	0.6	0.5	0.897674	0.0000900132	2.62876	0.00712403
		0.8	0.4	0.883782	0.0000641366	2.59859	0.00569431
	0.5	0.5	0.4	0.752469	0.0000234311	2.30749	0.00293049
			0.5	0.865533	0.0000461844	2.55785	0.00460621

**Table 4.** The relations of the thermo-physical properties of the nanofluids and hybrid nanofluids [1,8,16,17,56].

Properties	Nanofluid	Hybrid Nanofluid
Density ( $\rho$ )	$\rho_{nf} = (1 - \varphi) * \rho_f + \varphi\rho_s$	$\rho_{hnf} = \rho_f \left[ (1 - \varphi_2) \left[ (1 - \varphi_1) + \varphi_1 \left( \frac{\rho_{s1}}{\rho_f} \right) \right] + \varphi_2 \left( \frac{\rho_{s2}}{\rho_f} \right) \right]$
Viscosity ( $\mu$ )	$\mu_{nf} = \frac{\mu_f}{(1-\varphi)^{2.5}}$	$\mu_{hnf} = \frac{\mu_f}{(1-\varphi_1)^{2.5}(1-\varphi_2)^{2.5}}$
Heat capacity ( $\rho c_p$ )	$(\rho c_p)_{nf} = (1 - \varphi) * (\rho c_p)_f + \varphi * (\rho c_p)_s$	$(\rho C_p)_{hnf} = (\rho C_p)_f \left[ (1 - \varphi_2) \left\{ (1 - \varphi_1) + \varphi_1 \left[ \frac{(\rho C_p)_{s1}}{(\rho C_p)_f} \right] \right\} + \varphi_2 \left[ \frac{(\rho C_p)_{s2}}{(\rho C_p)_f} \right] \right]$
Electric conductivity ( $\sigma$ )	$\frac{\sigma_{nf}}{\sigma_f} = 1 + \frac{3(\sigma_s - \sigma_f)}{(\sigma_s - 2\sigma_f) - (\sigma_s - \sigma_f)\varphi}$	$\frac{\sigma_{hnf}}{\sigma_f} = 1 + \frac{3(\sigma_{s1}\varphi_1 - \sigma_{s2}\varphi_2)(\varphi_1 + \varphi_2)/\sigma_f}{2 + [(\sigma_{s1} + \sigma_{s2})/\sigma_f] - [(\sigma_{s1}\varphi_1 - \sigma_{s2}\varphi_2)/\sigma_f] + (\varphi_1 + \varphi_2)}$
Thermal conductivity (k)	$\frac{k_{nf}}{k_f} = \frac{(k_s + 2k_f) - 2*\varphi*(k_f - k_s)}{(k_s + 2k_f) + \varphi*(k_f - k_s)}$	$\frac{k_{hnf}}{k_{bf}} = \left( \frac{k_{s2} + (n-1)k_{bf} - (n-1)\varphi_2(k_{bf} - k_{s2})}{k_{s2} + (n-1)k_{bf} + \varphi_2(k_{bf} - k_{s2})} * \frac{k_{s1} + (n-1)k_f - (n-1)\varphi_1(k_f - k_{s1})}{k_{s1} + (n-1)k_f + \varphi_1(k_f - k_{s1})} \right)$

### 4. Results and Discussion

In this section, we discuss the outcomes of the magneto-hydrodynamic flow of different hybrid nanofluids (Ag-MoS<sub>2</sub>/H<sub>2</sub>O, Ag-MoS<sub>2</sub>/EO, Ag-MoS<sub>2</sub>/EG) under the effect of different study parameters, namely the magnetization force, thermal radiation, stretching, and rotational ratios. The local skin friction in the xy-direction, Nusselt and Sherwood number outcomes are presented in Tables 1–3, respectively. The thermophysical properties of the nanofluids and hybrid nanofluids are represented in Table 4. Additionally, Table 5 provides the numeric values of the different properties of nano-particles and base fluids utilized in this study. Furthermore, the outcomes of the study were validated with the already published results by Hussain et al. [56] and the agreement is presented in Table 6.

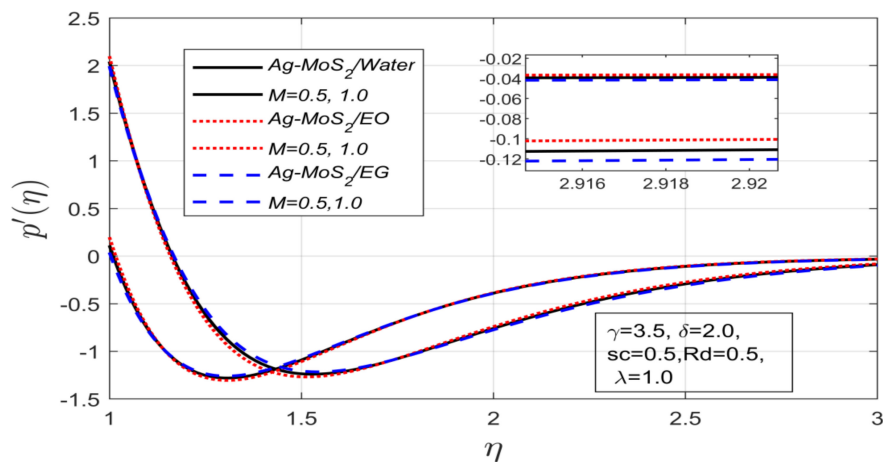
**Table 5.** The thermophysical properties of the nanoparticles and base fluids [1,2,8,16].

Physical Properties	Ag	MoS <sub>2</sub>	H <sub>2</sub> O	C <sub>2</sub> H <sub>6</sub> O <sub>2</sub>	EO
(Density) $\rho$	10,490	5060	997	1063	884
(heat capacity) $c_p$	235	397.21	4179	3630	1910
(Thermal conductivity) $k$	429	904.4	0.6130	0.387	0.144
(Prandtl number) $p_r$			6.2	203.20	6450

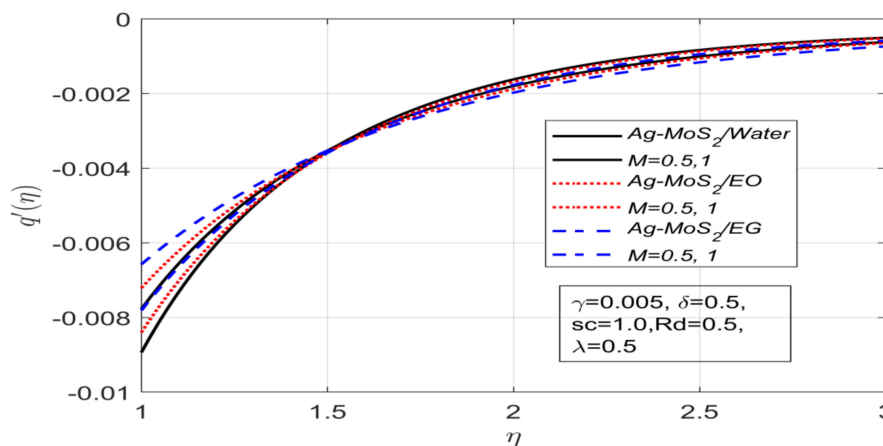
**Table 6.** A comparison of the Nusselt number of the present study under the nonlinear radiation effect with Hussain et al. [56].

$\varphi_1 = \varphi_2 = 0.1$		Present Results of Ag-MoS <sub>2</sub> /Water <i>Rd</i> = 1			Hussain et al. [56] <i>Rd</i> = 1	
M	$\lambda$	<i>Rd</i> = 0	$r_w = 1.1$	$r_w = 1.8$	$r_w = 1.1$	$r_w = 1.8$
1	0	2.33015	2.32658	2.60957	2.4653	2.88787
	0.5	2.32583	2.34789	2.60908	2.17291	2.39552
	1	2.32053	2.37409	2.64658	1.89916	2.03691
	2	2.31116	2.42038	2.77017	1.54042	1.64452

Figure 2a–d describes the impact of the magnetic field *M* on the primary, secondary velocities, temperature profile, and concentration profile, respectively. The primary velocity under increasing magnetic impact decreased (see Figure 2a), but the secondary velocity increased with the augmentation in magnetization force (see Figure 2b), because a strong magnetic field creates a Lorentz force, which acts as a resistive force for fluid flow motion. The temperature profile for hybrid fluids (Ag-MoS<sub>2</sub>/H<sub>2</sub>O and Ag-MoS<sub>2</sub>/EG) was improved even under the influence of the magnetic field and thermal radiation (see Figure 2c), but the temperature profile for the engine oil-based hybrid nanofluid (Ag-MoS<sub>2</sub>/EO) declined dramatically. The concentration profile under the increasing impact of magnetic force *M* increased for all three examined hybrid nanofluids (see Figure 2d). It is interesting to note here that the associated concentration layer thickness contracted for all of the explored cases of hybrid nanofluids.

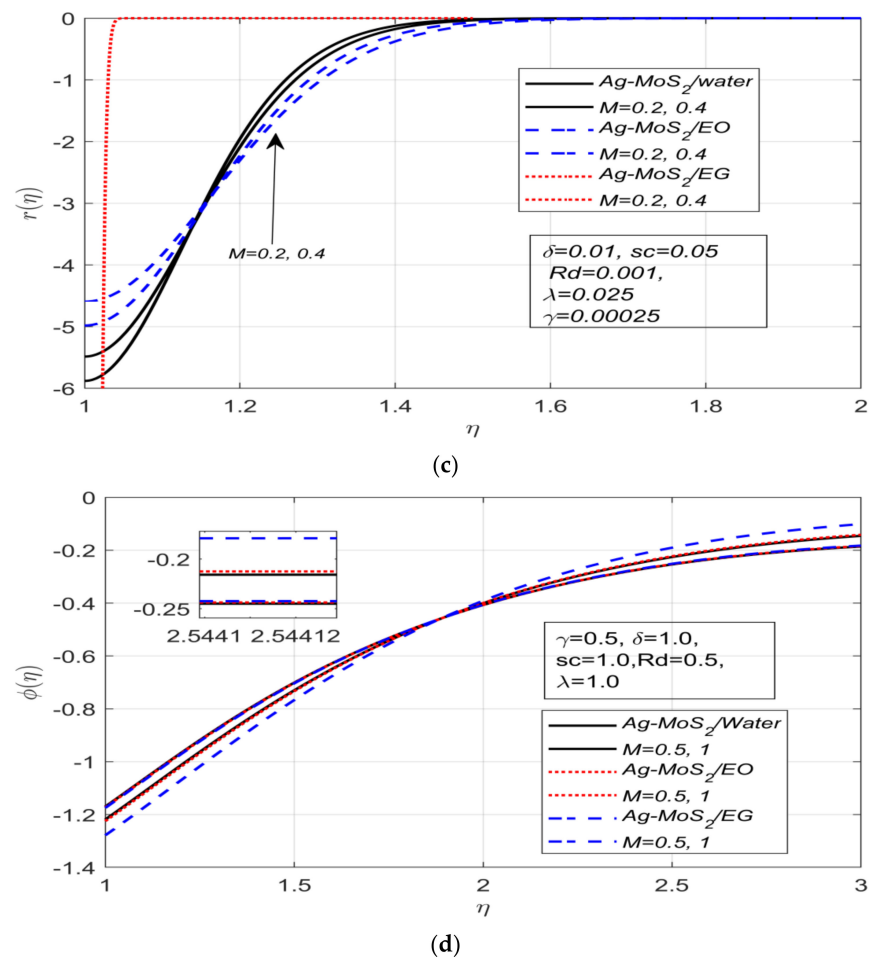


(a)



(b)

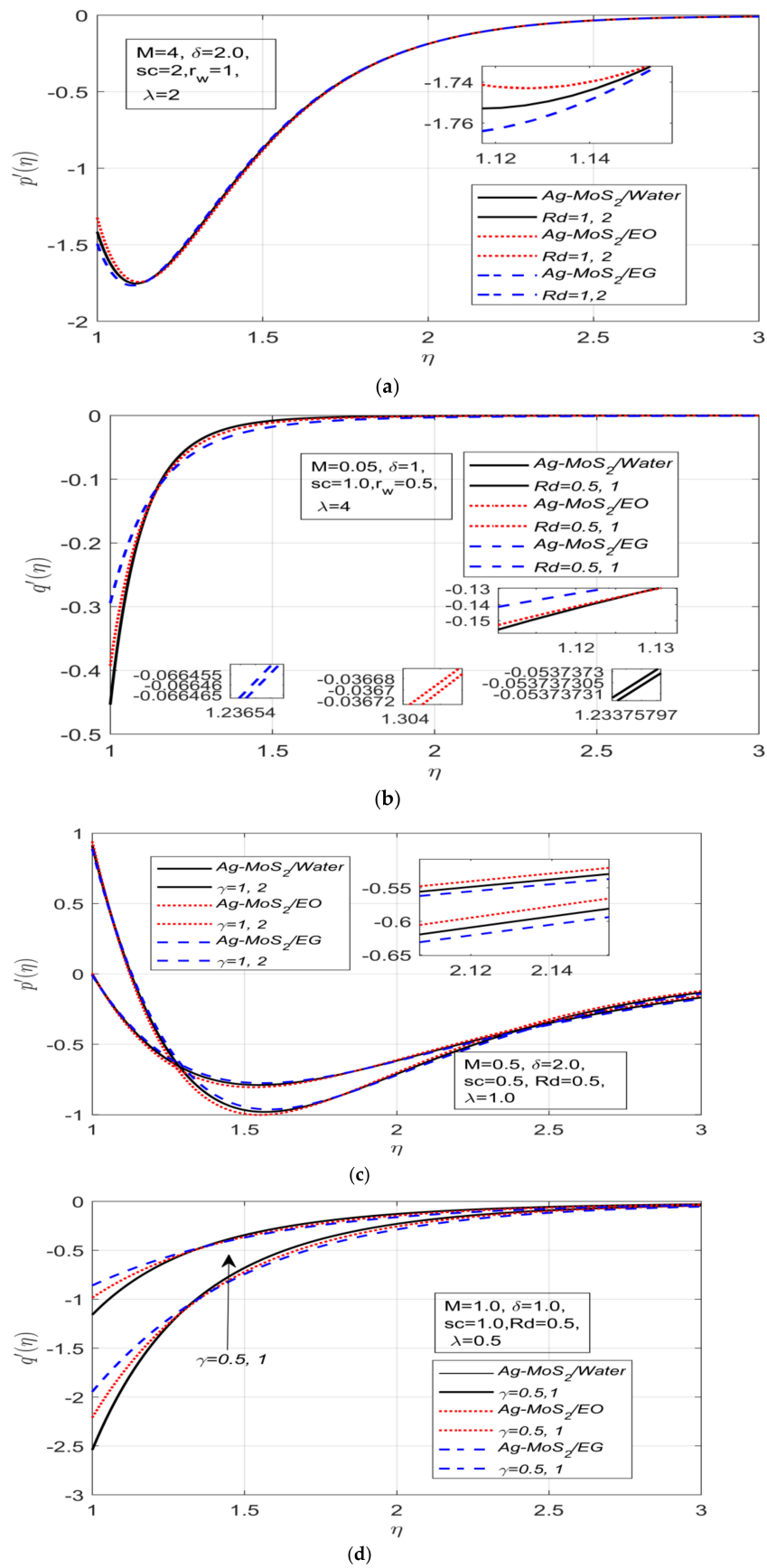
**Figure 2.** Cont.



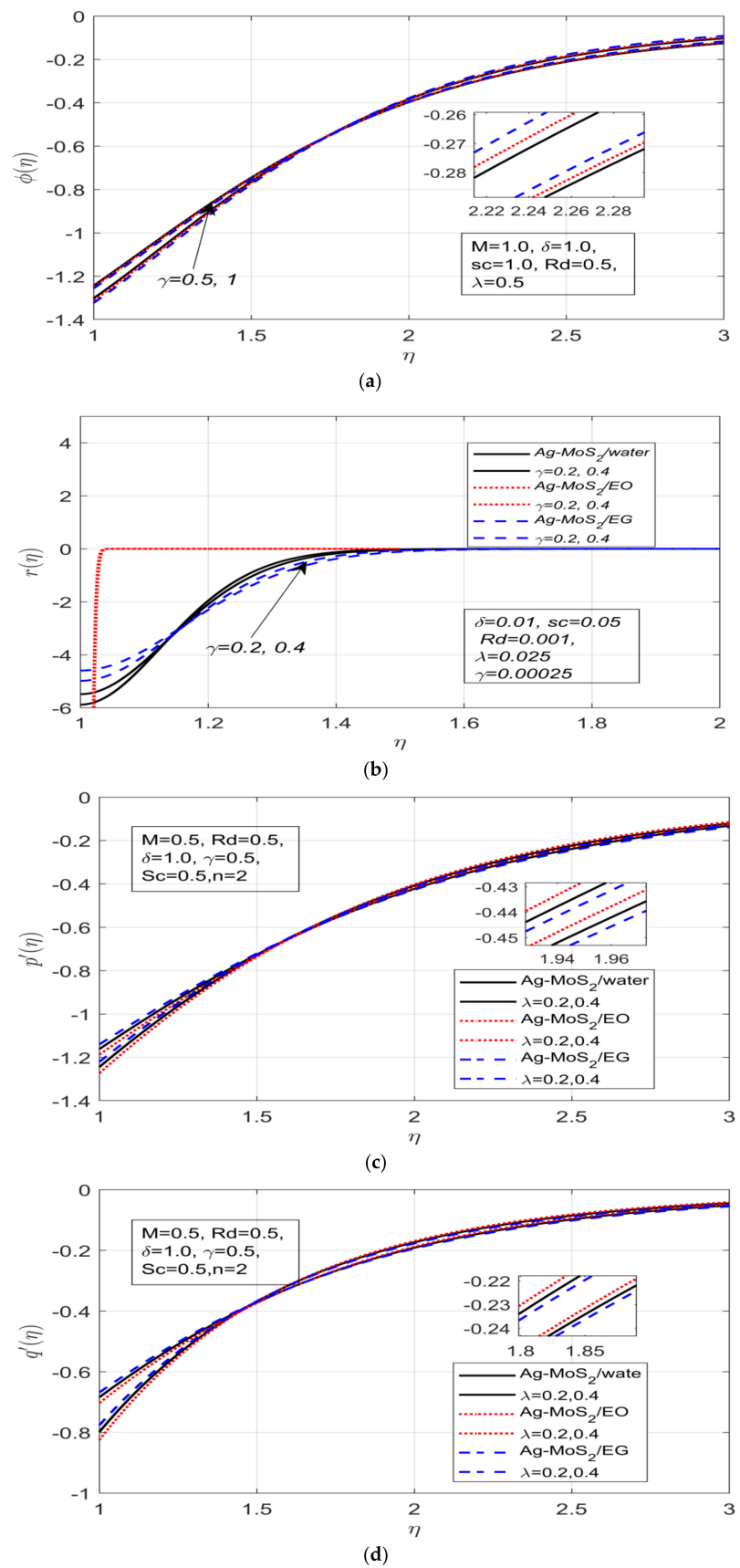
**Figure 2.** (a) The influence of  $M$  on the primary velocity  $p'$ . (b) The influence of  $M$  on the secondary velocity  $q'$ . (c) The impact of  $M$  on the temperature profile  $r$ . (d) The impact of  $M$  on the concentration profile  $\phi$ .

Figure 3a,b describes the influence of radiation  $Rd$  on the primary (see Figure 3a) and secondary (see Figure 3b) velocities. The increment in the radiation parameter increases the velocity for each explored hybrid nanofluid case. Consequently, the momentum layer thickness contracted dramatically. Figure 3c,d depicts the effect of the stretching ratio on primary and secondary velocities. The primary (see Figure 3c) and secondary (see Figure 3d) velocities both decreased and increased under the increasing influence of the stretching ratio, respectively. The concentration profile significantly increased as the stretching ratio increased due to the fact that stretching increases the thermal boundary layer of the fluid, resulting in an increase in the concentration profile in all three cases (see Figure 4a).

The effect of the stretching ratio on the temperature profile in three different cases is depicted in Figure 4b. The temperature profile increased for the Ag-MoS<sub>2</sub>/H<sub>2</sub>O and Ag-MoS<sub>2</sub>/EG hybrid nanofluids while it decreased for Ag-MoS<sub>2</sub>/EO with an increase in the stretching ratio. The rotation ratio affects the primary and secondary velocity profiles, as shown in Figure 4c,d. Figure 5a,b shows how the rotation parameter affects the temperature and concentration profiles, respectively. The velocity profiles increased under the increasing rotation parameter, resulting in a contraction in the momentum layer. Additionally, it was observed that contraction in momentum layer thickness enhanced rapidly in the secondary velocity profile compared to the primary profile. The temperature profile exhibited a very distinct behavior in all three cases, with the temperature profile for engine oil and ethylene glycol-based hybrid nanofluids actually increased, but drastically decreased for the water-based hybrid nanofluids (see Figure 5a). The concentration profile increased for all three distinct cases as the magnetic field and rotation parameter increased (see Figure 5b).



**Figure 3.** (a) The impact of radiation  $Rd$  on primary velocity  $p'$ . (b) The impact of radiation  $Rd$  on secondary velocity  $q'$ . (c) The impact of stretching ratio  $\gamma$  on the primary velocity  $p'$ . (d) The impact of stretching ratio  $\gamma$  on three secondary velocity  $q'$ .



**Figure 4.** (a) The impact of stretching ratio  $\gamma$  on the concentration profile  $\phi$ . (b) The impression of the stretching ratio  $\gamma$  on the temperature profile  $r$ . (c) The impact of rotation  $\lambda$  on the primary velocity  $p'$ . (d) The impact of rotation  $\lambda$  on the secondary velocity  $q'$ .

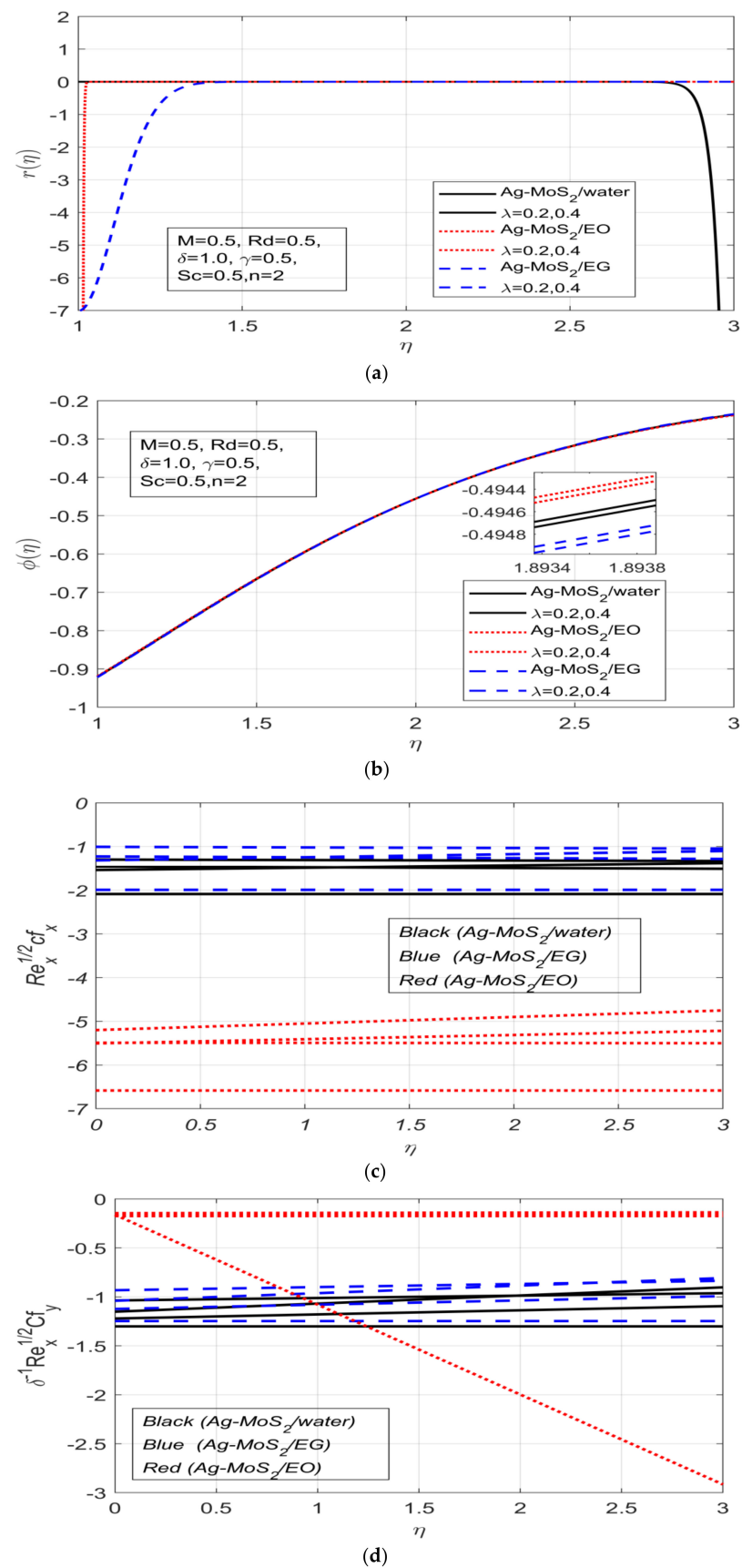


**Figure 5.** (a) The impact of rotation  $\lambda$  on the temperature profile  $r$ . (b) The impact of rotation  $\lambda$  on the concentration profile  $\phi$ . (c) The behavior of skin friction in the x-direction for three cases. (d) The behavior of skin friction in the y-direction for three cases.

Table 1 describes the skin friction results for three different cases under several study parameters. The increment in study parameter  $\delta$  showed a very slight impact on the skin friction in  $(Cf_x, Cf_y)$  for all three cases, which stayed consistent. The skin friction  $(Cf_x, Cf_y)$  under the influence of increasing magnetic parameter  $M$  was observed to increase for all three cases. The skin friction  $(Cf_x, Cf_y)$  under augmentation in the rotational ratio parameter  $\lambda$  decreased for all cases in  $(Cf_x)$ , but increased for  $(Cf_y)$ . The influence of increasing the stretching ratio  $\gamma$  was decreased skin friction in  $(Cf_x)$ , but increased in  $(Cf_y)$  for all of the study cases. Table 2 describes the Nusselt and Sherwood numbers under the influence of different study parameters. The maximum Nusselt number was observed under the increasing influence of the stretching ratio for Ag-MoS<sub>2</sub>/EO. The Nusselt number in Ag-MoS<sub>2</sub>/EG was slightly lower than in the case of Ag-MoS<sub>2</sub>/H<sub>2</sub>O. The maximum Sherwood number was observed in the Ag-MoS<sub>2</sub>/EO case and the minimum was observed for Ag-MoS<sub>2</sub>/EG. Figure 5c,d, and Figure 6 describe the graphical behavior of skin frictions  $(Cf_x, Cf_y)$  and Nusselt number  $(Nu_x)$  for all three cases under study, respectively, and the graphical data are provided in Tables 1 and 2 below.

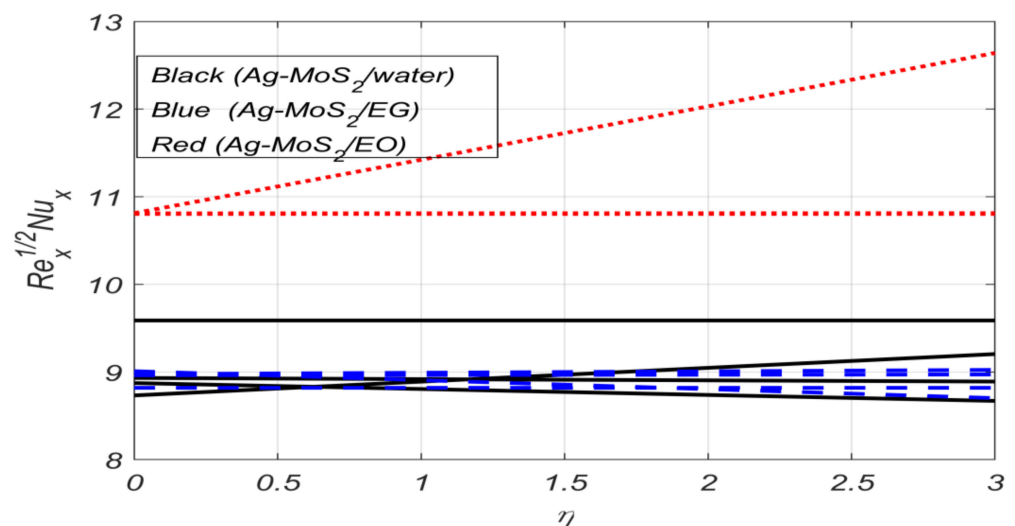


Figure 6. The behavior of the Nusselt number  $(Nu_x)$  for the three cases.

Table 3 shows the influence of nonlinear radiation on the heat transfer coefficient. The Nusselt number in the Ag-MoS<sub>2</sub>/H<sub>2</sub>O case was observed as the maximum even under the increasing influence of nonlinear radiation. The Nusselt number in the Ag-MoS<sub>2</sub>/EG case were found to be much lower compared to case 1 under nonlinear radiation, as the impact of nonlinear radiation could not be processed due to the presence of high pressure gradients. Table 4 presents the thermo-physical properties utilized for the nanoparticles and base fluids for the study analysis. Table 5 shows the numeric values for the different properties of the base fluids and nano-sized particles. Furthermore, the outcomes of the present study were validated with already published results by Hussain et al. [56] (see Table 6).

## 5. Conclusions

In the present study, the steady three-dimensional magneto-hydrodynamic flow of hybrid nanofluids under the effect of linear and nonlinear radiation was investigated over a stretching surface to analyze the heat and mass transfer attributes. The formulated problem was tackled with the BVP-4c technique in MATLAB. The outcomes of the study for the three examined hybrid nanofluids are presented graphically and discussed. Furthermore, the obtained results were validated by performing a comparison with the already published results. The notable outcomes of our study are listed as follows:

1. The momentum layer thickness decreased with an increment in the magnetization force, stretching, and rotational ratio whereas it improved with increased radiation.
2. Expansion was observed in the thermal boundary layer with an increasing influence of magnetization force and stretching ratio. The high rotational motion of flow contracted the thermal boundary of the rotating flow.
3. The concentration profile inclined with augmentation in magnetization, stretching, and rotational ratio. Additionally, the associated concentration layer contracted.
4. The minimum shear stress rates were observed for Ag-MoS<sub>2</sub>/EG in both the x and y directions. The contrast in the behavior of shear stress was demonstrated by the other examined hybrid nanofluids.
5. High heat and mass transfer coefficients were obtained under linear radiation impact for Ag-MoS<sub>2</sub>/EO and the minimum rates were obtained for Ag-MoS<sub>2</sub>/EG.
6. The Nusselt number showed an increasing trend with an increment in the nonlinear radiation parameter for the Ag-MoS<sub>2</sub>/water hybrid nanofluid.

### Future Research

In this work, we investigated the heat and mass transfer in magneto-hydrodynamic steady three dimensional rotating hybrid nanofluid flow. One can examine the combined effect of transverse magnetization and nonlinear radiation.

**Author Contributions:** Conceptualization, A.H. (Ali Hassan) and A.H. (Azad Hussain); methodology, A.H. (Ali Hassan).; software, A.H. (Ali Hassan).; validation, J.A., H.K. and F.M.A.; formal analysis, A.H. (Ali Hassan). And M.A.; investigation, J.A., W.P. and M.A.; resources, J.A. and W.P.; data curation, A.H. (Ali Hassan); writing—original draft preparation, A.H. (Ali Hassan); writing—review and editing, A.H. (Ali Hassan); visualization, H.K. and F.M.A.; supervision, A.H. (Azad Hussain); project administration, A.H. (Ali Hassan).; funding acquisition, J.A., W.P., H.K. and F.M.A. All authors have read and agreed to the published version of the manuscript.

**Funding:** This research received no external funding.

**Institutional Review Board Statement:** Not applicable.

**Informed Consent Statement:** Not applicable.

**Data Availability Statement:** The data can be made available by corresponding author following a request.

**Acknowledgments:** Princess Nourah bint Abdulrahman University Researchers Supporting Project number (PNURSP2022R192), Princess Nourah bint Abdulrahman University, Riyadh, Saudi Arabia.

**Conflicts of Interest:** Authors declare that they have no conflict of interest.

### Nomenclature

$u, v, w$	Velocities components in respective direction ( $\text{ms}^{-1}$ )
$\nu_f$	Kinematic viscosity of base fluid ( $\text{m}^2\text{s}^{-1}$ )
$\rho_f$	The density of base fluids ( $\text{kgm}^{-3}$ )
$C_p$	Heat capacity at constant pressure ( $\text{Jkg}^{-1}\text{K}^{-1}$ )
$\rho_{nf}$	Density of nano-particles ( $\text{kgm}^{-3}$ )
$\gamma$	Stretching ratio [–]
$Rd$	Radiation parameter [–]
$Re$	Reynolds number [–]
$Sh_x$	Sherwood number [–]
$Nu_x$	Nusselt number [–]
$\eta$	Similarity variable [–]
$C_W, C_\infty$	Surface and ambient concentration [–]
$(\alpha)_{hnf}$	Thermal diffusivity of hybrid nanofluids
$HNF$	Hybrid nanofluids
$EG$	Ethylene glycol

$(\rho c_p)_f$	Volumetric heat capacity of base fluid $(\text{JK}^{-1})$
$(\rho C_p)_{nf}$	Volumetric heat capacity of nanofluid $(\text{JK}^{-1})$
$T_W, T_\infty$	Surface and ambient temperature (K)
$\omega^*$	Rotational velocity of hybrid fluids
$\mu_f$	Dynamic viscosity $(\text{kgm}^{-1}\text{s}^{-1})$
$\lambda$	Rotational ratio of flow [–]
$M$	Magnetic field parameter [–]
$Pr.$	Prandtl number [–]
$Cf_x$	Skin Friction along the $x$ -axis [–]
$Cf_y$	Skin Friction along the $y$ -axis [–]
$r, \varphi$	Temperature and concentration profiles, respectively [–]
$p, q$	Primary and secondary velocities, respectively [–]
$D_m$	Mass diffusivity [–]
$EO$	Engine oil

## References

- Hussain, A.; Hassan, A.; Al Mdallal, Q.; Ahmad, H.; Rehman, A.; Altanji, M.; Arshad, M. Heat transport investigation of magneto-hydrodynamics (SWCNT-MWCNT) hybrid nanofluid under the thermal radiation regime. *Case Stud. Therm. Eng.* **2021**, *27*, 101244. [[CrossRef](#)]
- Mebarek-Oudina, F. Convective heat transfer of Titania nanofluids of different base fluids in cylindrical annulus with discrete heat source. *Heat Transfer—Asian Res.* **2018**, *48*, 135–147. [[CrossRef](#)]
- Marzougui, S.; Mebarek-Oudina, F.; Assia, A.; Magherbi, M.; Shah, Z.; Ramesh, K. Entropy generation on magneto-convective flow of copper–water nanofluid in a cavity with chamfers. *J. Therm. Anal.* **2020**, *143*, 2203–2214. [[CrossRef](#)]
- Shafiq, A.; Mebarek-Oudina, F.; Sindhu, T.N.; Abidi, A. A study of dual stratification on stagnation point Walters’ B nanofluid flow via radiative Riga plate: A statistical approach. *Eur. Phys. J. Plus* **2021**, *136*, 407. [[CrossRef](#)]
- Hussain, A.; Hassan, A.; Arshad, M.; Rehman, A.; Matoog, R.; Abdeljawad, T. Numerical simulation and thermal enhancement of multi-based nanofluid over an embrittled cone. *Case Stud. Therm. Eng.* **2021**, *28*, 101614. [[CrossRef](#)]
- Jamshed, W.; Devi, S.S.U.; Prakash, M.; Hussain, S.M.; Eid, M.R.; Nisar, K.S.; Muhammad, T. Entropy Amplified solitary phase relative probe on engine oil based hybrid nanofluid. *Chin. J. Phys.* **2022**, *77*, 1654–1681. [[CrossRef](#)]
- Ouni, M.; Ladhar, L.M.; Omri, M.; Jamshed, W.; Eid, M.R. Solar water-pump thermal analysis utilizing copper–gold/engine oil hybrid nanofluid flowing in parabolic trough solar collector: Thermal case study. *Case Stud. Therm. Eng.* **2022**, *30*, 101756. [[CrossRef](#)]
- Ghadikolaie, S.; Gholinia, M.; Hoseini, M.; Ganji, D. Natural convection MHD flow due to  $\text{MoS}_2$ –Ag nanoparticles suspended in  $\text{C}_2\text{H}_6\text{O}_2\text{H}_2\text{O}$  hybrid base fluid with thermal radiation. *J. Taiwan Inst. Chem. Eng.* **2019**, *97*, 12–23. [[CrossRef](#)]
- Hayat, T.; Nadeem, S. Heat transfer enhancement with Ag–CuO/water hybrid nanofluid. *Results Phys.* **2017**, *7*, 2317–2324. [[CrossRef](#)]
- Hayat, T.; Nadeem, S.; Khan, A.U. Rotating flow of Ag–CuO/H<sub>2</sub>O hybrid nanofluid with radiation and partial slip boundary effects. *Eur. Phys. J. E* **2018**, *41*, 1–9. [[CrossRef](#)]
- Ghadikolaie, S.; Hosseinzadeh, K.; Ganji, D. Investigation on ethylene glycol–water mixture fluid suspend by hybrid nanoparticles (TiO<sub>2</sub>–CuO) over rotating cone with considering nanoparticles shape factor. *J. Mol. Liq.* **2018**, *272*, 226–236. [[CrossRef](#)]
- Huminic, G.; Huminic, A. Hybrid nanofluids for heat transfer applications—A state-of-the-art review. *Int. J. Heat Mass Transf.* **2018**, *125*, 82–103. [[CrossRef](#)]
- Mebarek-Oudina, F.; Aissa, A.; Mahanthesh, B.; Öztop, H.F. Heat transport of magnetized Newtonian nanoliquids in an annular space between porous vertical cylinders with discrete heat source. *Int. Commun. Heat Mass Transf.* **2020**, *117*, 104737. [[CrossRef](#)]
- Marzougui, S.; Mebarek-Oudina, F.; Magherbi, M.; Mchirgui, A. Entropy generation and heat transport of Cu–water nanoliquid in porous lid-driven cavity through magnetic field. *Int. J. Numer. Methods Heat Fluid Flow* **2021**, *32*, 2047–2069. [[CrossRef](#)]
- Khan, U.; Zaib, A.; Mebarek-Oudina, F. Mixed convective magneto flow of  $\text{SiO}_2$ – $\text{MoS}_2$ /C<sub>2</sub>H<sub>6</sub>O<sub>2</sub> hybrid nanoliquids through a vertical stretching/shrinking wedge: Stability analysis. *Arab. J. Sci. Eng.* **2020**, *45*, 9061–9073. [[CrossRef](#)]
- Hassan, A.; Hussain, A.; Arshad, M.; Alanazi, M.M.; Zahran, H.Y. Numerical and Thermal Investigation of Magneto-Hydrodynamic Hybrid Nanoparticles (SWCNT-Ag) under Rosseland Radiation: A Prescribed Wall Temperature Case. *Nanomaterials* **2022**, *12*, 891. [[CrossRef](#)] [[PubMed](#)]
- Hassan, A.; Hussain, A.; Arshad, M.; Haider, Q.; Althobaiti, A.; Elagan, S.K.; Abdelmohimen, M.A. Heat transport investigation of hybrid nanofluid (Ag–CuO) porous medium flow: Under magnetic field and Rosseland radiation. *Ain Shams Eng. J.* **2022**, *13*, 101667. [[CrossRef](#)]
- Sidik, N.A.C.; Adamu, I.M.; Jamil, M.M.; Kefayati, G.H.; Mamat, R.; Najafi, G. Recent progress on hybrid nanofluids in heat transfer applications: A comprehensive review. *Int. Commun. Heat Mass Transf.* **2016**, *78*, 68–79. [[CrossRef](#)]
- Sundar, L.S.; Sharma, K.V.; Singh, M.K.; Sousa, A.C.M. Hybrid nanofluids preparation, thermal properties, heat transfer and friction factor—a review. *Renew. Sustain. Energy Rev.* **2017**, *68*, 185–198. [[CrossRef](#)]

20. Sarkar, J.; Ghosh, P.; Adil, A. A review on hybrid nanofluids: Recent research, development and applications. *Renew. Sustain. Energy Rev.* **2015**, *43*, 164–177. [[CrossRef](#)]
21. Huminic, G.; Huminic, A. Heat transfer capability of the hybrid nanofluids for heat transfer applications. *J. Mol. Liq.* **2018**, *272*, 857–870. [[CrossRef](#)]
22. Swain, K.; Mebarek-Oudina, F.; Abo-Dahab, S.M. Influence of MWCNT/Fe<sub>3</sub>O<sub>4</sub> hybrid nanoparticles on an exponentially porous shrinking sheet with chemical reaction and slip boundary conditions. *J. Therm. Anal.* **2021**, *147*, 1561–1570. [[CrossRef](#)]
23. Choi, S.U.; Eastman, J.A. *Enhancing Thermal Conductivity of Fluids with Nanoparticles* (No. ANL/MSD/CP-84938; CONF-951135-29); Argonne National Lab. (ANL): Argonne, IL, USA, 1995.
24. Jamshed, W.; Devi, S., S.U.; Safdar, R.; Redouane, F.; Nisar, K.S.; Eid, M.R. Comprehensive analysis on copper-iron (II, III)/oxide-engine oil Casson nanofluid flowing and thermal features in parabolic trough solar collector. *J. Taibah Univ. Sci.* **2021**, *15*, 619–636. [[CrossRef](#)]
25. Asogwa, K.K.; Mebarek-Oudina, F.; Animasaun, I.L. Comparative Investigation of Water-Based Al<sub>2</sub>O<sub>3</sub> Nanoparticles Through Water-Based CuO Nanoparticles Over an Exponentially Accelerated Radiative Riga Plate Surface via Heat Transport. *Arab. J. Sci. Eng.* **2022**, *47*, 8721–8738. [[CrossRef](#)]
26. Shahzad, F.; Jamshed, W.; Ibrahim, R.W.; Nisar, K.S.; Qureshi, M.A.; Hussain, S.M.; Isa, S.S.P.M.; Eid, M.R.; Abdel-Aty, A.-H.; Yahia, I.S. Comparative Numerical Study of Thermal Features Analysis between Oldroyd-B Copper and Molybdenum Disulfide Nanoparticles in Engine-Oil-Based Nanofluids Flow. *Coatings* **2021**, *11*, 1196. [[CrossRef](#)]
27. Sheikholeslami, M.; Ellahi, R. Three dimensional mesoscopic simulation of magnetic field effect on natural convection of nanofluid. *Int. J. Heat Mass Transf.* **2015**, *89*, 799–808. [[CrossRef](#)]
28. Majeed, A.; Zeeshan, A.; Alamri, S.Z.; Ellahi, R. Heat transfer analysis in ferromagnetic viscoelastic fluid flow over a stretching sheet with suction. *Neural Comput. Appl.* **2016**, *30*, 1947–1955. [[CrossRef](#)]
29. Zeeshan, A.; Majeed, A. Heat transfer analysis of Jeffery fluid flow over a stretching sheet with suction/injection and magnetic dipole effect. *Alex. Eng. J.* **2016**, *55*, 2171–2181. [[CrossRef](#)]
30. Hussain, A.; Hassan, A.; Al Mdallal, Q.; Ahmad, H.; Rehman, A.; Altanji, M.; Arshad, M. Heat transportation enrichment and elliptic cylindrical solution of time-dependent flow. *Case Stud. Therm. Eng.* **2021**, *27*, 101248. [[CrossRef](#)]
31. Nadeem, S.; Lee, C. Boundary layer flow of nanofluid over an exponentially stretching surface. *Nanoscale Res. Lett.* **2012**, *7*, 94. [[CrossRef](#)]
32. Raza, J.; Mebarek-Oudina, F.; Ram, P.; Sharma, S. MHD Flow of Non-Newtonian Molybdenum Disulfide Nanofluid in a Converging/Diverging Channel with Rosseland Radiation. *Defect Diffus. Forum* **2020**, *401*, 92–106. [[CrossRef](#)]
33. Raza, J.; Mebarek-Oudina, F.; Chamkha, A. Magnetohydrodynamic flow of molybdenum disulfide nanofluid in a channel with shape effects. *Multidiscip. Model. Mater. Struct.* **2019**, *15*, 737–757. [[CrossRef](#)]
34. Mebarek-Oudina, F. Numerical modeling of the hydrodynamic stability in vertical annulus with heat source of different lengths. *Eng. Sci. Technol. Int. J.* **2017**, *20*, 1324–1333. [[CrossRef](#)]
35. Chabani, I.; Mebarek-Oudina, F.; Ismail, A.A.I. MHD Flow of a Hybrid Nano-Fluid in a Triangular Enclosure with Zigzags and an Elliptic Obstacle. *Micromachines* **2022**, *13*, 224. [[CrossRef](#)]
36. Laouira, H.; Mebarek-Oudina, F.; Hussein, A.K.; Kolsi, L.; Merah, A.; Younis, O. Heat transfer inside a horizontal channel with an open trapezoidal enclosure subjected to a heat source of different lengths. *Heat Transf.—Asian Res.* **2020**, *49*, 406–423. [[CrossRef](#)]
37. Reddy, Y.D.; Mebarek-Oudina, F.; Goud, B.S.; Ismail, A.I. Radiation, Velocity and Thermal Slips Effect Toward MHD Boundary Layer Flow Through Heat and Mass Transport of Williamson Nanofluid with Porous Medium. *Arab. J. Sci. Eng.* **2022**, *47*, 1–15. [[CrossRef](#)]
38. Choudhari, R.; Makinde, O.D.; Mebarek-Oudina, F.; Vaidya, H.; Prasad, K.V.; Devaki, P. Analysis of third-grade liquid under the influence of wall slip and variable fluid properties in an inclined peristaltic channel. *Heat Transf.* **2022**, *51*, 2363–2861. [[CrossRef](#)]
39. Kataria, H.R.; Mistry, M.H. Entropy optimized MHD fluid flow over a vertical stretching sheet in presence of radiation. *Heat Transf.* **2021**, *51*, 2546–2564. [[CrossRef](#)]
40. Nadeem, S.; Fuzhang, W.; Alharbi, F.M.; Sajid, F.; Abbas, N.; El-Shafay, A.; Al-Mubaddel, F.S. Numerical computations for Buongiorno nano fluid model on the boundary layer flow of viscoelastic fluid towards a nonlinear stretching sheet. *Alex. Eng. J.* **2021**, *61*, 1769–1778. [[CrossRef](#)]
41. Hussain, A.; Arshad, M.; Rehman, A.; Hassan, A.; Elagan, S.; Alshehri, N. Heat Transmission of Engine-Oil-Based Rotating Nanofluids Flow with Influence of Partial Slip Condition: A Computational Model. *Energies* **2021**, *14*, 3859. [[CrossRef](#)]
42. Rasool, G.; Shafiq, A.; Hussain, S.; Zaydan, M.; Wakif, A.; Chamkha, A.J.; Bhutta, M.S. Significance of Rosseland’s Radiative Process on Reactive Maxwell Nanofluid Flows over an Isothermally Heated Stretching Sheet in the Presence of Darcy–Forchheimer and Lorentz Forces: Towards a New Perspective on Buongiorno’s Model. *Micromachines* **2022**, *13*, 368. [[CrossRef](#)] [[PubMed](#)]
43. Arshad, M.; Hussain, A.; Hassan, A.; Khan, I.; Badran, M.; Mehrez, S.; Elfassakhany, A.; Abdeljawad, T.; Galal, A.M. Heat Transfer Analysis of Nanostructured Material Flow over an Exponentially Stretching Surface: A Comparative Study. *Nanomaterials* **2022**, *12*, 1204. [[CrossRef](#)] [[PubMed](#)]
44. Makinde, O.D.; Khan, Z.H.; Ahmad, R.; Khan, W.A. Numerical study of unsteady hydromagnetic radiating fluid flow past a slippery stretching sheet embedded in a porous medium. *Phys. Fluids* **2018**, *30*, 083601. [[CrossRef](#)]
45. Reddy, M.V.; Lakshminarayana, P.; Vajravelu, K. A comparative study of mhd non-newtonian fluid flows with the effects of chemical reaction and radiation over a stretching sheet. *Comput. Therm. Sci. Int. J.* **2021**, *13*, 17–29. [[CrossRef](#)]

46. Vishalakshi, A.B.; Mahabaleshwar, U.S.; Sarris, I.E. An MHD Fluid Flow over a Porous Stretching/Shrinking Sheet with Slips and Mass Transpiration. *Micromachines* **2022**, *13*, 116. [[CrossRef](#)]
47. Ghadikolaie, S.; Hosseinzadeh, K.; Hatami, M.; Ganji, D. MHD boundary layer analysis for micropolar dusty fluid containing Hybrid nanoparticles (Cu-Al<sub>2</sub>O<sub>3</sub>) over a porous medium. *J. Mol. Liq.* **2018**, *268*, 813–823. [[CrossRef](#)]
48. Ghadikolaie, S.; Hosseinzadeh, K.; Ganji, D.; Hatami, M. Fe<sub>3</sub>O<sub>4</sub>-(CH<sub>2</sub>OH)<sub>2</sub> nanofluid analysis in a porous medium under MHD radiative boundary layer and dusty fluid. *J. Mol. Liq.* **2018**, *258*, 172–185. [[CrossRef](#)]
49. Raptis, A.; Perdakis, C.; Takhar, H. Effect of thermal radiation on MHD flow. *Appl. Math. Comput.* **2004**, *153*, 645–649. [[CrossRef](#)]
50. Nadeem, S.; Haq, R.; Lee, C. MHD flow of a Casson fluid over an exponentially shrinking sheet. *Sci. Iran.* **2012**, *19*, 1550–1553. [[CrossRef](#)]
51. Sarada, K.; Gowda, R.; Sarris, I.; Kumar, R.; Prasannakumara, B. Effect of Magnetohydrodynamics on Heat Transfer Behaviour of a Non-Newtonian Fluid Flow over a Stretching Sheet under Local Thermal Non-Equilibrium Condition. *Fluids* **2021**, *6*, 264. [[CrossRef](#)]
52. Mishra, S.; Khan, I.; Al-Mdallal, Q.; Asifa, T. Free convective micropolar fluid flow and heat transfer over a shrinking sheet with heat source. *Case Stud. Therm. Eng.* **2018**, *11*, 113–119. [[CrossRef](#)]
53. Abo-Dahab, S.M.; Abdelhafez, M.A.; Mebarek-Oudina, F.; Bilal, S.M. MHD Casson nanofluid flow over non-linearly heated porous medium in presence of extending surface effect with suction/injection. *Indian J. Phys.* **2021**, *95*, 2703–2717. [[CrossRef](#)]
54. Hamrelaine, S.; Mebarek-Oudina, F.; Sari, M.R. Analysis of MHD Jeffery Hamel flow with suction/injection by homotopy analysis method. *J. Adv. Res. Fluid Mech. Therm. Sci.* **2019**, *58*, 173–186.
55. Shafiq, A.; Mebarek-Oudina, F.; Sindhu, T.N.; Rassoul, G. Sensitivity analysis for Walters' B nanoliquid flow over a radiative Riga surface by RSM. *Sci. Iran.* **2022**, *29*, 1236–1249.
56. Hussain, A.; Elkotb, M.A.; Arshad, M.; Rehman, A.; Nisar, K.S.; Hassan, A.; Saleel, C.A. Computational Investigation of the Combined Impact of Nonlinear Radiation and Magnetic Field on Three-Dimensional Rotational Nanofluid Flow across a Stretchy Surface. *Processes* **2021**, *9*, 1453. [[CrossRef](#)]
57. Zainal, N.A.; Nazar, R.; Naganthran, K.; Pop, I. Unsteady EMHD stagnation point flow over a stretching/shrinking sheet in a hybrid Al<sub>2</sub>O<sub>3</sub>-Cu/H<sub>2</sub>O nanofluid. *Int. Commun. Heat Mass Transf.* **2021**, *123*, 105205. [[CrossRef](#)]
58. Chamkha, A.J.; Aly, A. Mhd free convection flow of a nanofluid past a vertical plate in the presence of heat generation or absorption effects. *Chem. Eng. Commun.* **2010**, *198*, 425–441. [[CrossRef](#)]
59. Farooq, S.; Khan, M.I.; Waqas, M.; Hayat, T.; Alsaedi, A. Transport of hybrid type nanomaterials in peristaltic activity of viscous fluid considering nonlinear radiation, entropy optimization and slip effects. *Comput. Methods Programs Biomed.* **2019**, *184*, 105086. [[CrossRef](#)]
60. Abbas, S.; Khan, W.; Waqas, M.; Irfan, M.; Asghar, Z. Exploring the features for flow of Oldroyd-B liquid film subjected to rotating disk with homogeneous/heterogeneous processes. *Comput. Methods Programs Biomed.* **2020**, *189*, 105323. [[CrossRef](#)]
61. Gangadhar, K.; Bhargavi, D.N.; Kannan, T.; Venkata Subba Rao, M.; Chamkha, A.J. Transverse MHD flow of Al<sub>2</sub>O<sub>3</sub>-Cu/H<sub>2</sub>O hybrid nanofluid with active radiation: A novel hybrid model. *Math. Methods Appl. Sci.* **2020**. [[CrossRef](#)]
62. Hosseini, S.; Ghasemian, M.; Sheikholeslami, M.; Shafee, A.; Li, Z. Entropy analysis of nanofluid convection in a heated porous microchannel under MHD field considering solid heat generation. *Powder Technol.* **2018**, *344*, 914–925. [[CrossRef](#)]
63. Sheikholeslami, M.; Jafaryar, M.; Li, Z. Second law analysis for nanofluid turbulent flow inside a circular duct in presence of twisted tape turbulators. *J. Mol. Liq.* **2018**, *263*, 489–500. [[CrossRef](#)]